Granular Matter 1, 83–91 © Springer-Verlag 1998

Simulation of the pressure distribution under a two-dimensional heap of polygonal particles

Hans-Georg Matuttis

Abstract Granular heaps in two dimensions are studied using the molecular dynamics method with convex polygons. The angle of repose shows a dependence on the size dispersion of the particles. There is a pressure minimum under the apex of the heap which depends strongly on the way the heap is built. The results and the comparisons with the experiments suggest that there is not such a thing as a generic pressure distribution for granular heaps.

1 Introduction

Over the last years, the pressure distribution under sand heaps has become a crucial issue in the research in static granular materials. A concise overview over the field has been given by Savage in [1] and in [2]. There are analytical [3–6] and semianalytical [7] results for the pressure distribution under sand heaps with a fixed base which show no minimum under the apex of the heap for non-deformed bases. Simulations of soft particles show basically the analytical results with slightly rounded curves [8, 9] even if the force laws are modified [10] and frictional non-spherical particles [11] are used. Pre-stressing the bottom of the pile may lead to pressure minima [9], but cannot explain quantitatively the marked pressure dip which has been found experimentally in [12] and [13].

This paper focuses on the effects of the (mesoscopic) particles on the macroscopic properties of the heap. The simulations presented in this paper use polygonal particles instead of round particles, incorporate properties like friction and size polydispersity and take into account boundary conditions like the flat base.

2 Experimental results on the pressure distribution

There are several, mostly experimental papers in the engineering literature on the pressure under heaps and wedges from the 1960's to the beginning of the 1980's. We follow the terminology of Savage [1], so that "cone" denotes a round heap, whereas "wedge" denotes a lengthy, extended heap of granular material (see Fig. 2). The papers accessible to the author on granular wedges were [14, 15], the papers on granular cones were [12] and [13]. We will discuss the relevance of two-dimensional simulations for the interpretation of three-dimensional experiments later in this paper.

The experimental results for wedges [14, 15] are consistent and show no pressure dip, independent of how the heap was built. The cones in the experimental literature [12, 13] all exhibit a marked pressure dip, and were all built in the wedge sequence.

To be consistent with the engineering literature, we normalize the normal stresses in units of $g\rho h$, the product of the height of the heap with the density of the material.

2.1 The geometry and history of the setup

There are different methods to build a heap of granular matter. We adopt the terminology of ref. [14], where the way to build a cone/wedge from a point source is called "wedge sequence", whereas a layer-wise construction is termed "layered sequence".

Fig. 1a denotes the layered sequence. The sketch for the wedge sequence in ref. [14], see Fig. 1b is misleading, because it does not scale with the shape of the growing heap. The ideal situation which can be scaled is sketched in Fig.1c, the realistic situation in 1d. The increasing size of the avalanches for increasing system size leads to a mixture of the strata in the foot of the heap and to asymmetries in the strata. This was found as a result of the simulations.

2.2 The experiment by Jotaki et al.

Jotaki et al. [12] measured the pressure distribution for four different materials: Sea Sand, Rape Seed and two kinds of sand named GB 708 and GB 733. The results show a dip in the pressure distribution which is smallest for rape seed, the material with the narrowest size distribution (for the distributions, see Table 1). The pressure is plotted in Fig. 3 for different sizes of the heap during the construction. The dip is shallower compared with the heap made from for the polydisperse sea sand (4). The smallest heap (height 3.3 cm) shows no dip due to the size

Received: 14 January 1998

H.-G. Matuttis
ICA 1 Universität Stuttgart, Pfaffenwaldring 27,
D-70569 Stuttgart, Germany
hg@ica1.uni-stuttgart.de

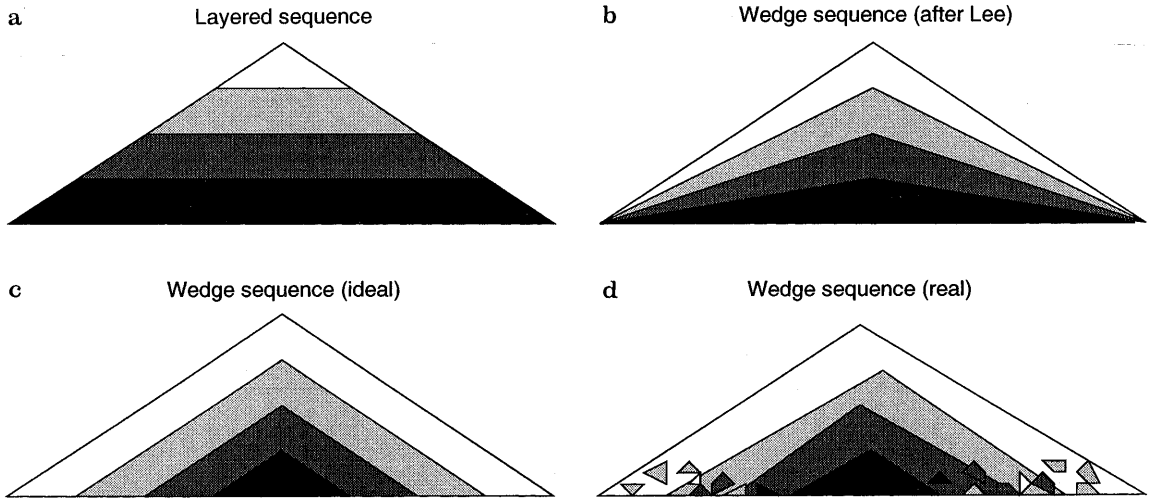

Fig. 1a–d. Sketch of the layered sequence (**a**) and the wedge sequence (**b–d**). Lighter shade indicates partilces which where poured on later in time

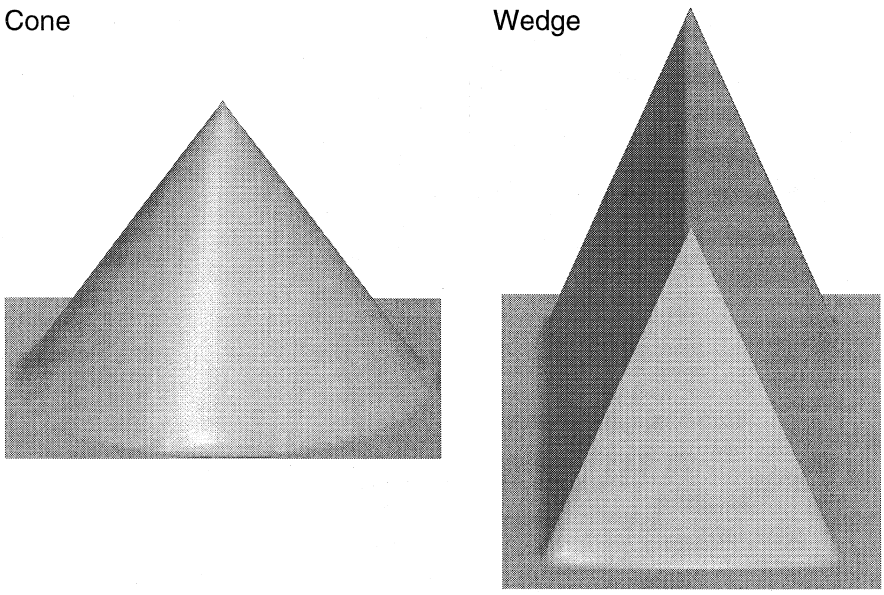

Fig. 2. Sketch of granular cones and granular wedges

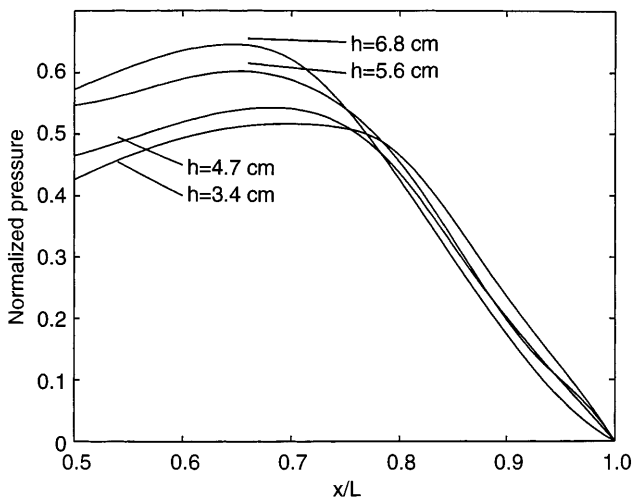

Fig. 3. Pressure distribution for a heap of rape seed from ref. [12]

of the pressure gauge. The size of the heaps ranges from 12 to 36 cm diameter, depending on the material.

The pressure gauge in the experiment of Jotaki et al. [12] had a diameter of 2 cm, so that it had nearly the sizeof the pressure dip for the small heaps. In the table 1, we give the minimal percentage of the pressure in the middle of the dip, the angle of repose, the particle size and the coefficient of internal friction. In the paper, the

Table 1. Parameters for the heaps in [12]

Material	Pressure Dip [%]	Angle of repose [deg]	Particle size [mm]	Coeff. of int. friction
GB 708	81	22.5	0.3–0.7	0.41
GB 733	60	22.7	0.044–0.088	0.27
Sea sand	77	33.6	0.17–0.71	0.6
Rape seed	87	24.9	1.4	0.40

Table 2. Verification of the pressure measurements in [13]. The largest derivations occur for heaps which are larger than the maximum distance of the pressure gauges. The data are averaged from the left and right half of the original plot and interpolated linearly for the integration

	Values for fertilizer:					Values for sand:				
height (in cm)	20	30	40	50	55	20	30	40	50	55
mass_h (in kg)	20	67	159	310	413	32	108	257	501	667
mass_s (in kg)	20	65.2	154	309	397	33	111	255	436	606
$\text{mass}_h/\text{mass}_s$	1	1.03	1.03	1.01	1.04	0.97	0.97	1	1.16	1.1

graphs are plotted only for the right half of the heap. The data are reproduced here because the original article is not easily accessible.

A common property of the pressure distribution is, that the tangent of the pressure is not flat in the middle of the heap, and that the scaled pressure distribution changes curvatures in the outer region for different heights. It is not possible to collapse the graphs on top of each other by scaling the normal stresses in units of $g\rho h$. From the paper of Jotaki et al., we can not decide whether this is a result of the large dimension of the used gauges, the impact height, the size of the feeder or still another effect.

2.3 The experiments by Smid and Novosad

The experiment by Smid and Novosad [13] was performed with sand and fertilizer. Regrettably, neither the grain size nor the diameter of the strain gauge was given. The measurements contain notable pressure asymmetries, whereas Jotaki et al. [12] plotted only one half space of the experiment. Nevertheless, assuming that the fertilizer used is the commercially available fertilizer ($d \approx 3$–5 mm), the dimensions in units of the grain diameter are comparable to the ones by Jotaki et al. [12].

Savage [1] computed the total weight from the given stresses by curve-fitting and integrating the data and found them to be 10% lower than the pile weight. He therefore argued that the accuracy the experiment by Smid and Novosad is questionable. No data or figures are given in [1], so we present the result of our calculations here. If one computes the masses of the heaps, first as given by the pile-height, angle of repose and density (mass_h) and second by integration of the stresses (mass_s), one obtains the values in table 2 for the fertilizer data and the sand data. Our data were obtained by integration of the linearly interpolated original data. It is not advisable to fit the data with higher order polynomials, because this leads easily to spurious negative pressures in the last measurement interval at the foot of the pile, so that the total computed mass may be grossly underestimated.

In table 2, there are large systematic deviations from the computed to the measured total weight for the high heaps of sand. They are nevertheless not very significant,

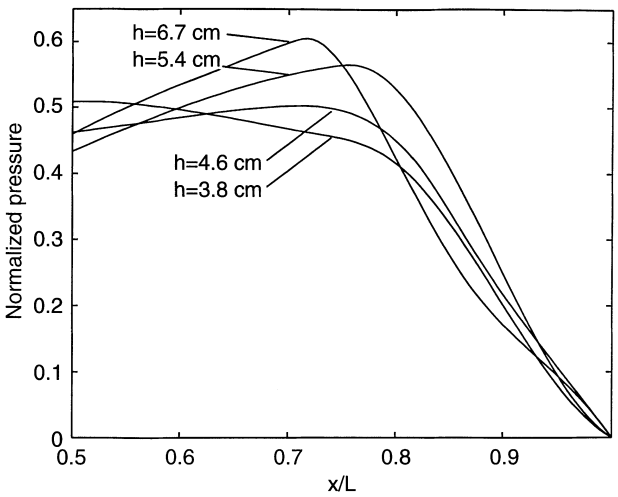

Fig. 4. Pressure distribution for a heap of sea sand from [12]

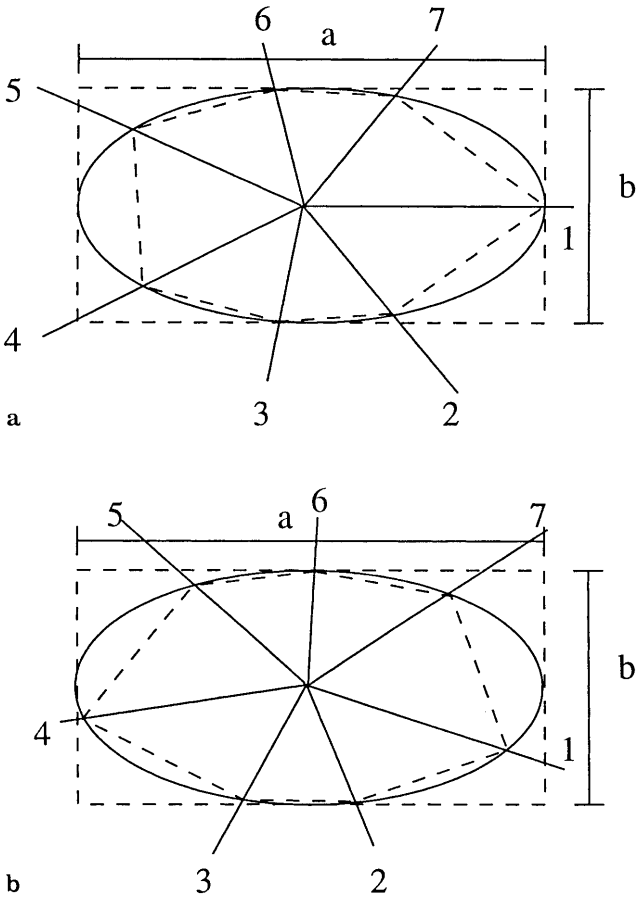

Fig. 5a,b. Construction method for polygons by inscribing them to ellipses with axes **a** and **b**. Different starting points 1 for the first edge lead to a slight polydispersity of the shape, but not of the area of the particles

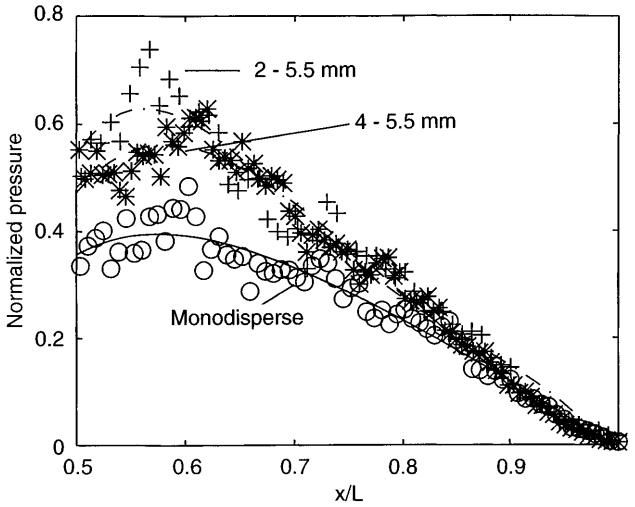

Fig. 6. Graph for the pressure distribution in the 2-dimensional heaps built in the wedge sequence

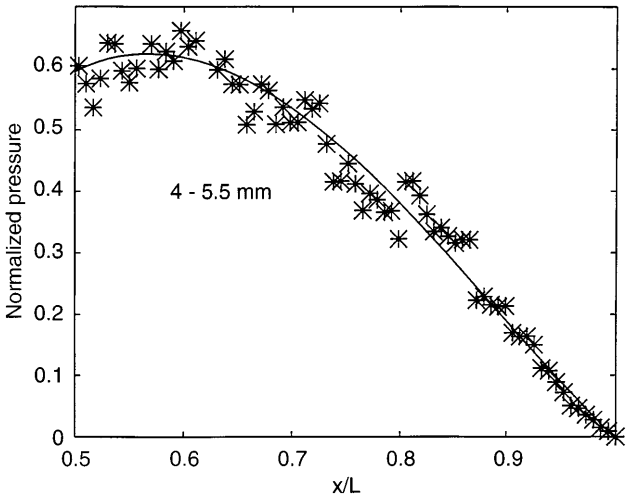

Fig. 7. Graph for the pressure distribution in the 2-dimensional heap built in the layered sequence

because the base diameter of the heaps is in that case already larger than the largest distance of the pressure gauges. That means, that the part of the heap with the largest radius and therefore a large contribution to the total weight does not show up in the measurement, so that the strongest deviations are possibly due to lack of data rather than to error-prone measurements. At least the data for the fertilizer seem to be consistent. In this respect, there is no reason to doubt that the pressure minimum in the experiments both by Jotaki et al. [12] and by Smid et al. [13] show a pressure dip for a cone on a flat base. There is no indication that the dip is the result of the deformation of the base as suggested by Savage [1].

As the precise coefficients of friction and particle size of the materials in [13] are not given, we will focus mainly on the data of [12].

3
The simulation

The numerical algorithmic details of the molecular dynamics simulation are described in Appendix A.

3.1
Setting up the simulation

In the simulation, irregular heptagons were used, which were inscribed to an ellipse with different axes. The irregularity was introduced by changing the starting point on the ellipse for the monodisperse particles, whereas the length of the axis of the ellipses were changed for the polydisperse particles (see Fig. 5).

The two dimensional density was 5000 kg/m^2, the modulus of elasticity was $1 \cdot 10^7$ N/m. We used a friction coefficient of $\mu = 0.6$ for the particle-particle and the particle-wall friction and a time-step between $dt = 10^{-5}$ s and $dt = 2.5 \cdot 10^{-5}$ s depending on the minimal particle radius.

Particles were dropped from 40 cm height with 0.2 m/s initial velocity. This large height was chosen to guarantee almost constant impact velocity throughout the simulation.

3.2
Wedge sequence

To suppress the fluctuations, we averaged horizontally over at least 12 neighboring particles along the bottom of the heap and averaged the measurements over the left and the right half of the system. The ground was flat in all simulations.

In Fig. 6 representative data are shown. Additional runs with different seeds gave equivalent results within the fluctuations. The data are fitted to a fourth order polynomial to guide the eyes. The size of the pressure dip is comparable to the pressure dip in the experiments. The number of particles per measurement interval was chosen depending on the total system size and the fluctuations in the system.

3.3
Layered sequence

The layered sequence was build with particles which were dropped from the height of less than 1 particle diameter onto the already present layers.

Settling effects in the strata of the system are strongly visible in Fig. 8. The pressure data in Fig. 7 are again fitted to a polynomial of fourth order to guide the eyes. There are two striking features of the outcome: The angle of repose in Table 4 is larger than for the wedge sequence with the same size distribution. This means, that in two dimensions the impact of the particles affects the angle of repose considerably. Moreover, in contrast to the three-dimensional experiment, the pressure distribution of the layered sequence in Fig. 7 differs strongly from the pressure under a wedge sequence in Fig. 6 with the same size distribution. For the layered sequence, only a very small dip is observed.

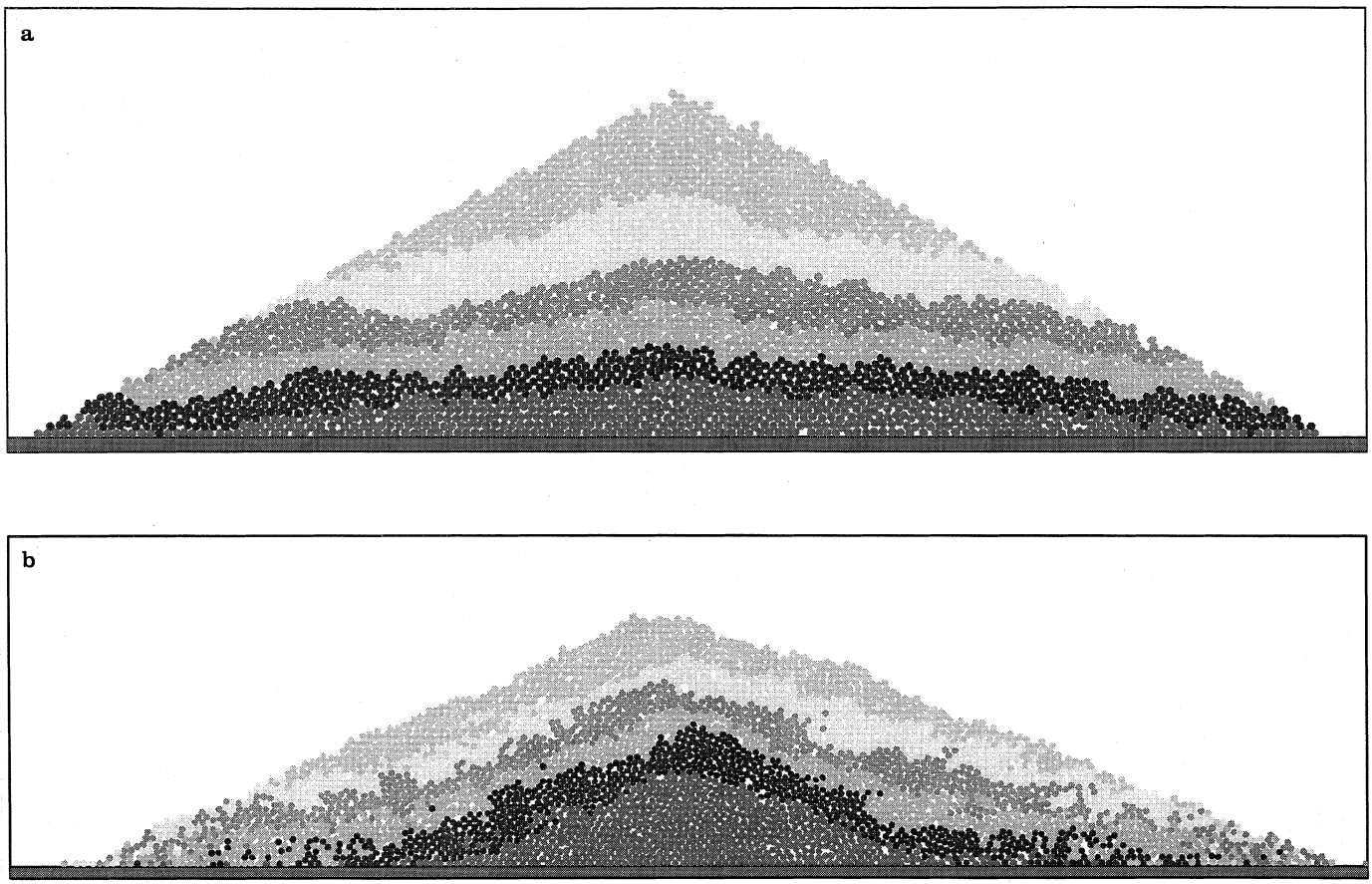

Fig. 8a,b. Konfiguration for the monodisperse layered sequence (**a**) and the polydisperse wedge sequence (**b**). Different shading indicates different age of the particles

4
Discussion of the simulation results and the experiments

4.1
Wedges and cones

The small size or even absence of the dip for the layered sequence is consistent with the experiments on wedges [14, 15], which do not exhibit a dip.

The small magnitude or absence of the dip for monodisperse systems even in a wedge sequence is consistent with the numerical model in [7], the calculation in [3] and the simulations in [6, 8, 10].

4.2
Consequences of system size and dimensionality

When one compares the size of two-dimensional simulations with three-dimensional measurements, one should compare the linear dimensions of the systems in units of particle diameters, not the total number of particles in a heap.

In Jotaki et al. [12], the grain size given for rape seed is 1.4 mm, with the base diameter of the largest heaps being 120 mm to 320 mm, so there were about 100 to 140 particles in the base of the smallest systems. In [13], the base length of the heap varies from 600 mm to 1700 mm for fertilizer, which has a grain size of about 3 to 5 mm, which also leads to a system size of 100 to several hundred particles. The simulations use also 120 to 140 particles in horizontal direction, so that the base length is comparable to the experimental heaps in units of the particle diameter.

The data from the experiments, especially the ones by Jotaki, are much smoother than the ones from the simulations, because the three-dimensional heaps are measured with two-dimensional pressure-gauges. Asymetries can be still observed in the data in ref. [13]. In the two-dimensional simulation, data can be collected only in one dimension, so that the number of particles in the simulation per measurement points is of the order of 10 instead of 10 by 10, nearly one order of magnitude less than in the experiments.

There is a fundamental difference in the geometry of two and three dimensions which affects the force propagation in granular materials. Two straight lines always intersect in two dimensions, but not in three dimensions. Therefore, the intersection of strong "branches" of a contact network may shift portions of material in two-dimensional simulations, but not in three-dimensional experiments.

In two-dimensional systems, the particles order more easily on a regular grid than in three dimensions. Stronger polydispersity destroys the ordering and thereby reduces the fluctuations.

Table 3. Parameters for the heaps built in a wedge sequence. For increasing polydisperse material, the angle of repose increases

Angle of rep. [deg]	Particle size $a \times b$ [mm]	Heap height [cm]	Particle tot./per bin
23	4 × 5	14	2600 / 14
24	4 × 4–5.5	17	4000 / 15
28	2–5.5 × 2–5.5	8	2000 / 12

Table 4. Parameters for the heap built in the layered sequence

Angle of rep. [deg]	Particle size $a \times b$ [mm]	Heap height [cm]	Particle tot./per bin
32	4 × 4–5.5	17	3400 / 10

4.3 Size dispersion

One of the most striking results of the experiments of Jotaki et al. [12] is, that for polydisperse Materials the pressure under the apex of the heap is about 20% to 30% smaller than at the maximum pressure. This occurs in granular materials with very different properties, like internal friction and critical angle (see table 1). It should also be noted, that the angles of repose range from 22.5° to 33.6°, while the coefficients of internal friction ranges from 0.27 to 0.61, but angle of repose and internal friction are not necessarily proportional, as can be seen from table 1. Polydisperse material was also used in the measuements of Smid et al. [13]. The only data from cones for which the minimum pressure was less than 15 % smaller than the maximum pressure was found for monodisperse rape seed.

This is consistent with the simulations presented in this paper, where the dip is more pronounced for polydisperse systems. The angle of repose increases with the polydispersity of the system (see table 3). The size of the pressure dip is comparable to the pressure dip in the experiments. The angle of repose seems to increase with the polydispersity of the system. The flat ground and the different size of the dip show that there was no effective bending due to the elasticity of the material which would account for a dip by an effective deformation of the ground.

5 Conclusion

The experiments on granular cones show the tendency that the dip in the pressure distribution increases with the amount of polydispersity of the granular material. Wedges, on the contray, do not show a dip because they are built layerwise in at least one direction.

The simulations presented in this paper reproduce the experimental findings and confirm, that the pressure distribution in a heap is no static property, but depends strongly on the history of the heap. There is an increase of the dip for stronger polydisperse material in heaps build in the wedge-sequence. The dip is practically absent for heaps built in a layered sequence.

Therefore, one can say that there are no "generic" sand heaps and no "generic" pressure distributions, but the macroscopic properties of the sand heaps are stongly affected by the grain properties of the heap. Continuum models and their boundary conditions always have to be specified for a specific kind of heap.

Monodisperse systems have shown the smallest dips in different setups, so that one can assume that the regular ordering in monodisperse systems inhibits arching mechanisms.

In the next step, the quantitative relation between the particle shape, friction coefficient, angle of repose, the size dispersion of the grains, the dropping height on the one hand and the angle of repose and the pressure distribution on the other hand has to be clarified more systematically.

I would like to thank Keiko Aoki for providing me with the original paper of Jotaki et al. [12]. Useful discussions with Stefan Luding, Tom Schanz and Alex Schinner are gratefully acknowledged.

Appendix A Modeling of polygonal granular materials

A contact force similar to the one in [16] for soft particle simulations with static friction [17] was implemented. Both the non-spherical particle shape and the static friction are crucial to allow the realistic build-up of the heap on a flat surface.

The basis of the molecular dynamics simulation are Newton's equations of motion for the translatory and rotatory degrees of freedom. Though a special choice of the force laws is outlined below, the details and the value of the parameters can be modified without changing the qualitative outcome of the simulations.

In the following, we outline the force law for the contact and the damping normal to the direction of the contacts and the tangential Coulomb friction force with realistic friction coefficients.

A.1 General considerations

The **direction** of the normal force is normal to the line which connects the intersection points. This direction is unique as long as there is no intersection between two "spikes" (triangles with very small angle).

The **force point** S_{ij} (see Fig. 9) is given as the middle of the intersection line of the two overlapping polygons. All relative velocities (normal and tangential are also computed with respect to this force point.

A.2 Fast overlap computation

To compute the overlap of two particles, it is necessary to compute the intersection of their boundary. This intersection is computed in several stages to save CPU-Time.

1. We treat only particles with angles equal or larger 90°.
2. The easiest way to exclude non-overlapping sides is the comparison of the x- and y-coordinates. Sides which cannot overlap are not treated in the following stages.

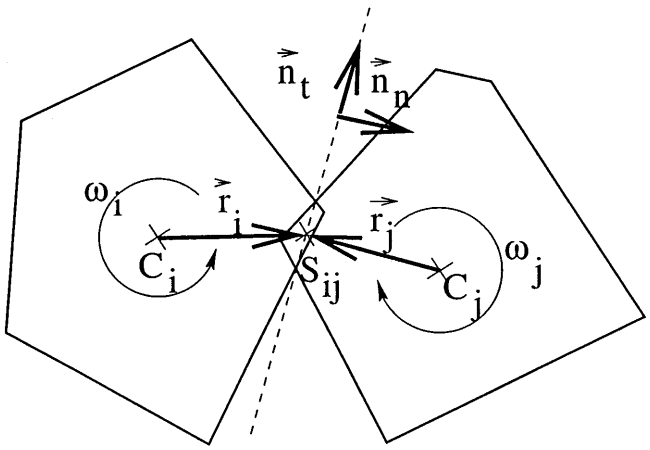

Fig. 9. Sketch of the geometry of a particle-particle contact for the polygonal simulation

3. To find out, whether two straight lines $[AB]$ and $[CD]$ intersect, it is enough to check the orientation of the triangles ABC, ABD, CDA and CDB. If ABC, ABD and CDA, CDB have pairwise opposite orientation, the lines intersect, see Fig. 10. The orientation is the sign of the cross product of two 2-dimensional vectors and can be computed in 3 FLOPs (FLOating Point operations). Therefore, the intersection can be checked with 12 FLOPs. In 50% of the cases, already the first pair of triangles will have equal sign, to that on average only 9 FLOPs are needed.
4. As we are only treating convex polygons with obtuse angles, the intersection detection can be stopped if two pairs of intersecting lines have been found.
5. For the computation of the intersection points, a 2 by 2 linear system of equations must be solved. Most of the computation time for that task is used for the necessary division, which takes about 50 times longer than a multiplication or an addition on a modern super-scalar workstation.
6. After the detection of the intersecting sides and their intersection point, the intersection area can be computed.

A.3 Normal forces

All the forces in this section are supposed to act in the normal direction of the particle contacts.

A.3.1 Contact force

Two overlapping particles are imagined to deform in such a way, that the overlap area is a measure of the deformation and thus is an estimate for the force between the two particles. Due to the reduced dimensionality (2D instead of 3D) one has to relate the particles to a certain length, which can be imagined as the length of rods in 3 dimensions, which form a 2-dimensional physical system.
The contact force $F_{c,\perp}$ is therefore proportional to

– the area A of the overlap between the two particles in units of [m^2].

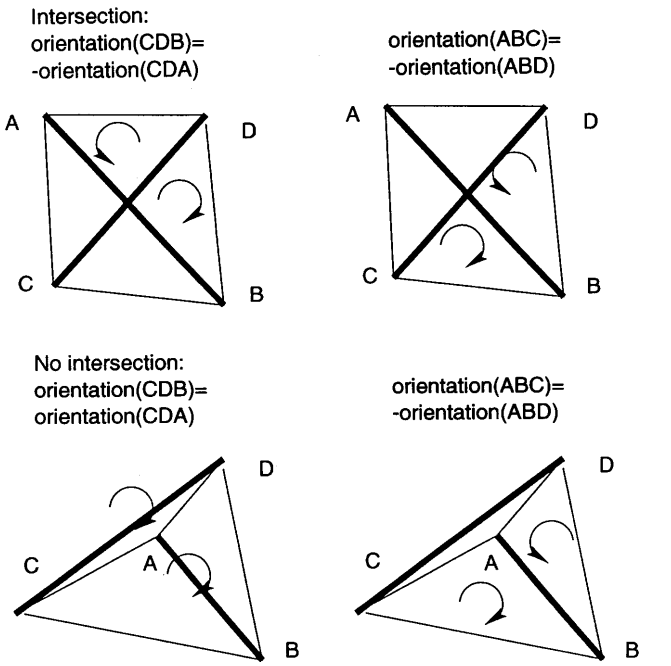

Fig. 10. Oriented triangles for intersection computation of straight lines

– the "Young's modulus" Y: The harder the particles are, the larger is the force of the particle if the overlap increases. Young's Modulus in 3 Dimensions has the unit $[N/m^2]$, in 2D one has therefore $[N/m]$.
– the inverse of the characteristic length l, which depends on the distance between the centers of mass and the force point l_1 and l_2

$$\frac{1}{l} = \frac{l_1 + l_2}{l_1 \cdot l_2}$$

This models the fact that the larger the particles are, the easier is the compression of a given area.

The resulting forcelaw is then $F_{c,\perp} = Y \cdot A/l$.

A.3.2 Damping force

The damping force $F_{c,\perp}$ leads to energy dissipation in normal direction. It is modeled like the damping in the harmonic oscillator and is proprotional to

– the square-root of the reduced mass of the two-particle system (analogous to the harmonic oscillator),
– the square-root of Young's modulus Y (analogous to the harmonic oscillator),
– to the change of the contact area per time $\mathrm{d}A/\mathrm{d}t$,
– to the damping constant $\gamma_\perp$, which gives the strength of the damping,
– to the inverse of the characteristic length l.

Comment It is also possible to compute the change of the contact area as the product of the normal velocity and the contact length. Due to the fact that the velocity in the numerical integration is the numerical derivative, which is stronger contaminated by fluctuations, we dit not use the velocity in the expression for the damping.

The damping term in normal direction is then

$$F_{d,\perp} = \begin{cases} Y \cdot \frac{\mathrm{d}A}{\mathrm{d}t}/l, & \text{for approach} \\ \max\left(Y \cdot \frac{\mathrm{d}A}{\mathrm{d}t}/l, -F_{c,\perp}\right) & \text{for separation} \end{cases}$$

Comment In the harmonic oscillator, the harmonic motion of the particle does not allow arbitrarily high velocities with zero amplitude, so that the potential is always smooth. In the modeling of grain contacts, there is a discontinuous force jump if the particle impacts with very high velocity. That may lead to the unphysical (in comparison to the un-damped oscillator) situation that the force on the particle is not largest when the overlap is largest, but when the relative velocities are largest.

For separating particles, one has to implement that the (attractive) damping cannot become larger than the (repulsive) contact force. This would lead to unphysical oscillations of the separating particles. A similar reasoning can be found in [18] for contact-mechanics simulations.

A.4 Tangential force

The tangential force acts as friction force normal to the Damping force in the same force point and perpendicular to the contact. It is again modeled like the harmonic oscillator. It is *incremented* proportional to

- the change in position since the previous contact $\Delta x = v_t \cdot \Delta t$,
- the tangential Young modulus $Y_t = Y \cdot 2/7$, which yields Coulomb friction for 2-particle contacts of round particles in a diluted granular system. The important aspect is that the normal and the tangential force are acting on the same time scale.

The tangential force is *truncated* at $F_\perp \cdot \mu$ with the coefficient of friction μ with $F_\perp = F_{d,\perp} + F_{c,\perp}$. Currently we do not discriminate between static and dynamic friction. The above system corresponds to a harmonic oscillator as long as no cut-off occurs. It is also necessary to include a damping in tangential direction to avoid undamped tangential oscillations. The tangential force is therefore proportional to

- the relative tangential velocity v_t,
- to the square root of the tangential Young's modulus $Y_t = Y * 2/7$. Y_t is chosen in such a way that for a diluted granular system the behavior for tangential collisions with Coulomb friction is recovered [19].
- the square root of the tangential mass (where the effect of the momenta of inertia I_1, I_2 have to be added to the reduced mass):
  $$m_{eff,\parallel} = \frac{1}{1/m_1 + 1/m_2 + r_1^2/I_1 + r_1^2/I_2}$$
- After adding the tangential damping, the resulting force must again be checked weather it is not larger than the Coulomb friction.

So the tangential force is

$$F_{d,\parallel}(t) = F_{d,\parallel}(t - \Delta t) + Y_t \cdot v_t \cdot \Delta t + \sqrt{m_{eff,\parallel} \cdot Y_t} v_t$$

if the normal force $F_{d,\parallel}(t) \leq \mu \cdot F_\perp$, else it is $\mu \cdot F_\perp$

A.5 Torques

The torques M are computed directly as the vector product of the forces $\mathbf{F}$ and the vectors $\mathbf{r}$ between center of mass and force points with

$$M = \mathbf{r} \times \mathbf{F}.$$

The torques are then inserted into the equation of motion for the momenta of inertia

$$M = I\dot{\omega}$$

A.6 Time Integration

We use the Gear predictor corrector formula of 5th order. Allen and Tildesly [20] recommend the application of only one single corrector step for the computer simulation of liquids, where smooth inter-particle potentials like the Lennard-Jones potential are used. As our inter-particle forces are not smooth, we use two predictor steps for a more stable treatment of the discontinuous contact forces. The higher order Gear predictor corrector schemes also do not suffer from the strong local fluctuations which are introduced by Verlet-like integration schemes. For a predictor-corrector-scheme with two corrector iterations, the typical time step for $\gamma_n = .5$ which can be used is about

$$\mathrm{d}t = 0.1\sqrt{m/Y} \cdot \pi$$

where m is the mass of the lightest particle and Y is the Young modulus. The high order of the integration scheme allows to choose the contact time in such a way that about 3 time steps during the approach and 3 time steps during the separation If there are less time steps the simulation becomes unstable.

Sometimes researchers find that they have to specify time-steps which are a factor of a hundred smaller than the theoretical contact times for the particles to prevent the simulation from becoming unstable. This results if no cutoff is used for the damping force, so that the resulting oscillations have a much smaller time scale than the actual collision.

A.7 Performance

The algorithm is written to simulate densely packed granular systems. For moderately polydisperse systems, the required CPU-time is proportional to the particle number. Walls are simulated as large particles, but are treated with a different neighborhood routine, so that the bottom of the system is simulated as one single particle. This excludes artefacts due to the joining of small particles like increases roughness due to additional normal force components.

One particle update costs about 90 μs on a Sparc Ultra (140 MHz) or a AIX PowerPC (120 MHz). As the corrector is applied twice, the force calculation has also to be applied twice. The time for the overlap computation lies between 25 % (IBM XLF-Compiler) and 45 % (SUN F90 Compiler) of the total execution time.

References

1. S.B. Savage: in Powders & Grains 97, edited by R.P. Behringer and J.T. Jenkins (Balkema, Rotterdam, 1997), pp. 185–194
2. Physics of dry granular media - NATO ASI Series, edited by H.J. Herrmann, J.-P. Hovi, and S. Luding (Kluwer Academic Publishers, Dordrecht, 1998)
3. D.C. Hong: Phys. Rev. E 47, 760 (1993)
4. G. Oron and H.J. Herrmann: Phys. Rev. E (1997), cond-mat/9707243
5. J.M. Huntley: Phys. Rev. E 48, 4099 (1993)
6. K. Liffman, D. Chan, and B.D. Hughes: Powder Technol. 78, 263 (1994)
7. D.H. Trollope and B.C. Burman: Géotechnique 30, 137 (1980)
8. K. Liffman, D.Y.C. Chan, and B.D. Hughes: Powder Technology 72, 255 (1992)
9. S. Luding, Phys. Rev. E 55, 4720 (1997)
10. S. Luding and H.-G. Matuttis: in Friction, Arching and Contact Dynamics, edited by D.E. Wolf and P. Grassberger (World Scientific, Singapore, 1997), pp. 373–376
11. H.-G. Matuttis and S. Luding: in Friction, Arching and Contact Dynamics, edited by D.E. Wolf and P. Grassberger (World Scientific, Singapore, 1997)
12. T. Jotaki and R. Moriyama: Journal of the Society of Powder Technology, Japan 16, 184 (1979)
13. J. Smid and J. Novosad: I. Chem. E. Symposium Series 63, D3/V/1 (1981)
14. J.H.I.K. Lee: Proceedings of the first Australian-New Zealand Conference on Geomechanics: Melbourne 1, 291 (1971)
15. B. Lackinger: Mitteilungen des Instituts für Bodenmechanik, Felsmechanik und Grund bau an der Fakultät für Bauingenieurwesen und Architekture der Universität Innsbruck 4, 1 (1980)
16. H.-J. Tillemans and H.J. Herrmann: Physica A 217, 261 (1995)
17. P.A. Cundall and O.D.L. Strack: Géotechnique 29, 47 (1979)
18. C.G.F. Pfeiffer: Multibody Dynamics with unilateral contacts, Wiley p28 f (1997)
19. J. Schäfer, S. Dippel, and D.E. Wolf: J. Phys. I France 6, 5 (1996)
20. M.P. Allen and D.J. Tildesley: Computer Simulation of Liquids (Oxford University Press, Oxford, 1987)